Sensors and Materials, Vol. 18, No. 7 (2006) 381–393
MYU Tokyo

S & M 0657

Experimental Study on Squeeze Film Damping of Perforated Micromechanical Structures Oscillating Perpendicular to the Substrate

Eung-Sam Kim, Ki-Ho Han, Young-Ho Cho* and Moon-Uhn Kim[1]

Digital Nanolocomotion Center, Korea Advanced Institute of Science and Technology,
373-1 Guseong-dong, Yuseong-gu, Daejeon 305-701, Korea
[1]Department of Mechanical Engineering, Korea Advanced Institute of Science and Technology,
373-1 Guseong-dong, Yuseong-gu, Daejeon 305-701, Korea

(Received July 11, 2006; accepted September 29, 2006)

Key words: microdamping, squeeze film damping, perforated plate, matched-asymptotic-expansions, edge effect

In this study, we investigate the squeeze film damping of a perforated planar micromechanical structure that oscillates in the normal direction to the substrate. We focus on the experimental data regarding the squeeze film damping compared with theoretical models based on matched-asymptotic-expansions, in terms of the size and number of perforations. A set of ten different structures, having three different sizes and different numbers of perforations, has been fabricated and tested. The experimental *Q*-factors, measured from the fabricated structures, are compared with two different theoretical values, estimated by finite element analysis (FEA) and matched-asymptotic-expansions. It is found that FEA overestimates the experimental values of the *Q*-factors by up to 150%. This major discrepancy is caused by the inaccuracy of the zero pressure boundary condition along the perforated edges. The values obtained from the matched-asymptotic-expansions, assuming nonzero pressure along the edges of the plates, are in good agreement with the experimental values within 20% margin of error.

1. Introduction

Recently, planar microstructures oscillating perpendicular to substrates (Fig. 1) have been widely used in microelectromechanical devices, such as microphones,[(1)] microaccelerometers[(2,3)] and tunable microoptical interferometers.[(4,5)] The micromechanical dynamics of perpendicularly oscillating planar structures are strongly governed by the viscous damping of the squeeze fluid medium. The significance of squeeze film damping increases when the micromechanical response of planar microdevices is controlled over a

*Corresponding author, e-mail address: nanosys@kaist.ac.kr

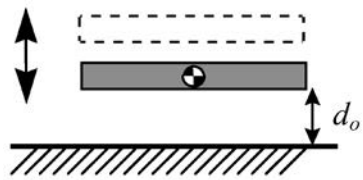

Fig. 1. Cross-sectional view of vertically oscillating planar microstructure.

wide frequency range or at resonance. Thus, a clear understanding and suitable specifications of squeeze film damping are important in the design of a wide bandwidth or resonant microstructures.

Extensive studies on squeeze film damping have been performed by Starr,[3] Sadd and Stiffler,[6] Blech,[7] and Andrews et al.[8] They have focused on the viscous damping and compressible spring effect of the fluid layer confined between parallel unperforated plates. Most surface-micromachined planar microstructures, however, are fabricated in the form of perforated plates to etch the underlying sacrificial layers and to reduce the squeeze film damping effect.

Recently, the squeeze film damping of perforated plates has been analyzed by Novack[2] and Kim et al.[9] using the finite element method (FEM) and by Kim et al.[10] using the matched-asymptotic-expansion method. In the finite element analysis (FEA),[2,9] the squeeze film damping of the perforated plates was evaluated using the conventional squeeze damping theory with zero pressure boundary conditions along perforation edges. In matched-asymptotic-expansion, however, the slow viscous flow due to the oscillating motion of the perforated plates was considered when the distance between the substrates and the perforated plates was much smaller than the characteristic dimensions of the plates.

In this study, we measured the incompressible squeeze film damping of unperforated and perforated plates. We have designed ten different damping structures, including a unperforated plate structure (Fig. 2) and nine perforated plate structures (Fig. 3), having different types of perforation in an equivalent damping area. We fabricated the test structures by two-layer polysilicon surface micromachining and compared the measured results with the estimated results from FEA (Appendix A.2) and matched-asymptotic-expansion (Appendix A.3). The discrepancy between the measured damping factors and the estimated results is discussed.

2. Perforated Plates and Test Structures

2.1 *Test structure design*

Figure 2 shows a damping test structure (H0), in which two pairs of folded microflexures (Table 1) support a unperforated square plate. We also consider square perforated plates (H1, H4, and H9) with square holes (Fig. 3) to characterize the effect of the perforation on squeeze film damping.

The size and number of square perforations in Fig. 3 satisfy the following conditions: 1) the net damping area of the perforated plates should be identical to that of the unperforated plate, 80×80 μm^2; 2) the plates in each row of Fig. 3 are required to have a constant area

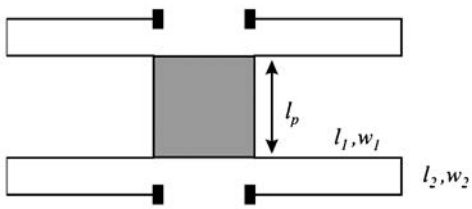

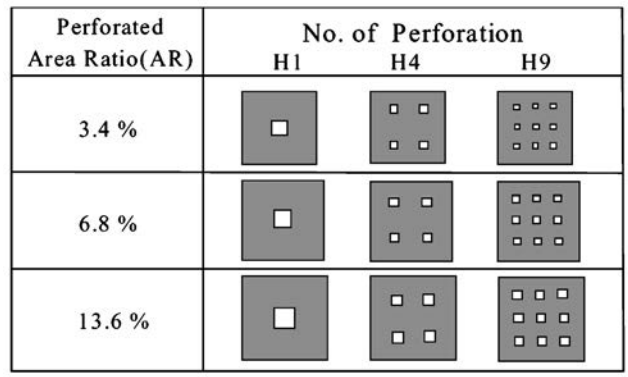

Fig. 2 (left). Top view of unperforated square plate, H0, suspended by two pairs of folded microflexures.
Fig. 3 (right). Perforated square plates with different sizes and numbers of holes. The outer area, A_{total}, and the sizes and numbers of perforation have a given area ratio, *AR*, at a fixed effective damping area, A_{eff}, of 6400 μm^2, where $A_{eff} = (A_{total}–A_{hole})$ and $AR = A_{hole}/A_{total}\times100\%$.

Table 1
Dimensions of microstructure of Fig. 2.

l_p	l_1	w_1	l_2	w_2
80 μm	311 μm	4 μm	32 μm	12 μm

ratio (*AR*), defined as

$$AR(\%) = \frac{N_h l_h^{\,2}}{l_o^{\,2}} \times 100, \tag{1}$$

where N_h, l_h, and l_o are the numbers of perforated holes, the hole size, and the outer edge length of the plate, respectively. The test structures in Fig. 3 have three different *AR* values of 3.4, 6.8, and 13.6%, respectively. An identical center-to-center distance separates the perforated holes. For the plates in each row of Fig. 3, which have identical *AR* values, the edge length of the outer plate is fixed whereas the edge lengths of the inner holes increase by factors of two and three successively in the row direction. For the plates in each column of Fig. 3, which have the same number of holes, both the outer edge length and the inner edge length increase as *AR* increases in the column direction.

The effective stiffness of four double-folded tethers in the vertical direction, k_{sq}, is

$$k_{sq} = \frac{4EI_1}{l_1^3}\left(\frac{1}{\left(\frac{2}{3} - \lambda + \frac{1-\lambda}{\alpha} + \frac{1}{\beta_1} + \frac{1}{3\beta_2}\right)}\right), \tag{2}$$

where $I_1 = (t^3 w_1/12)$ is the moment of area of beam 1; t, w_1, and l_1 are the thickness, width, and length of beam 1, respectively. Other symbols in eq. (2) are defined as $\alpha = GK_2/EI_1$, $\beta_i = GK_i/EI_i$, and $\lambda = (\alpha+1)/(2\alpha+1)$, where $K_i = (t_i^3 w_i/3)\{1–0.627(t_i/w_i)\tanh(\pi t_i/2w_i)\}$. The effective mass of the test structure, suspended from two pairs of double-folded tethers, is

$$m_{e,sl} = m_p + \frac{1754}{3360} m_1 + \frac{1}{4} m_2, \tag{3}$$

where m_p is the mass of the plate; m_1 and m_2 are the masses of the beams 1 and 2, respectively.

2.2 *Microfabrication*

The test structures are fabricated by six-mask, two-layer, polysilicon surface-micromachining, as shown in Fig. 4.

The process begins with the phosphorus doping of 4-inch, n-type (100) silicon wafers, using $POCl_3$ as the dopant source. Next, a 1-μm-thick thermal silicon dioxide (SiO_2) layer and a 0.2-μm-thick low pressure chemical vapor deposition (LPCVD) silicon nitride (Si_3N_4) layer are deposited as electrical isolation layers. Reactive ion etching (RIE) of the nitride/oxide sandwich layer is performed for the contact on the doped ground layer, as shown in Fig. 4(a). LPCVD of a 0.2-μm-thick polycrystalline silicon layer (1st poly) is followed by phosphorus doping performed at 970°C for 30 min, resulting in a sheet resistance of 5.27 Ω/□. The polysilicon electrodes are defined by RIE, as shown in Fig. 4(b). A 2-μm-thick sacrificial PSG layer is deposited on the wafer (Fig. 4(c)). In Fig. 4(d), a 4.3-μm-thick undoped polycrystalline silicon layer is deposited by LPCVD at 622°C after the removal of the native oxide in the contact area between the first and the second polysilicon layers. After the deposition of a 1.5-μm-thick PSG layer (Fig. 4(d)), an annealing is performed at 1000°C for 2 h not only to release the residual stress of the polysilicon layer, but also to obtain a symmetric diffusion of phosphorus onto the surface of the second polysilicon layer. After the PSG patterning, RIE using Cl_2 plasma (Fig. 4(e)) anisotropically etches the polysilicon structural layer. After the removal of the sacrificial PSG layer using a BOE solution, the wafer is rinsed and dried. To reduce adhesion, the wafer is rinsed in isopropyl alcohol and dried using an infrared lamp. The process is completed by the lift-off fabrication of a titanium-gold pad for wire bonding (Fig. 4(f)). The lift-off process uses PR as a mask material and titanium as an adhesive material for the gold evaporated by e-beam. Figure 5 shows a set of the microfabricated test structures with unperforated and perforated plates.

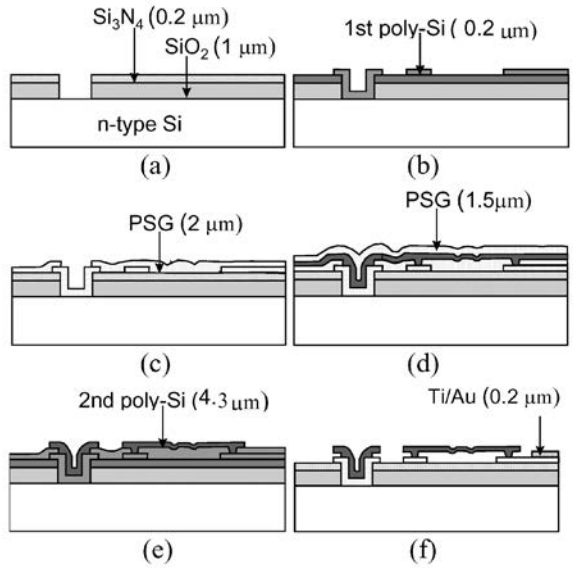

Fig. 4. Microfabrication of test structures.

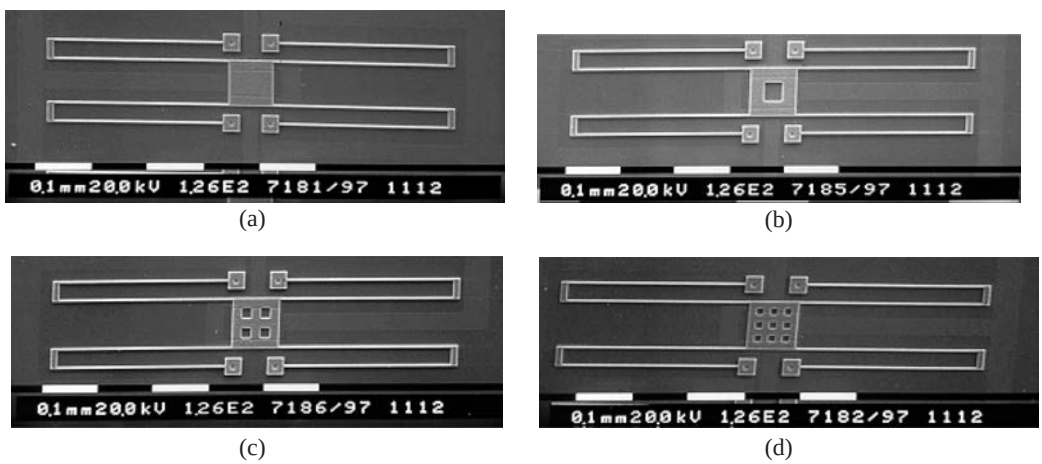

Fig. 5. Microfabricated test structures: (a) unperforated plate; (b)–(d) perforated plates.

3. Experimental Results and Discussion

For the squeeze film damping measurement, the planar microstructures were actuated electrostatically using an AC drive voltage of 18 V peak-to-peak amplitude. The velocity response of the planar microstructures was measured using a Mach-Zehnder interferometer as shown in Fig. 6.

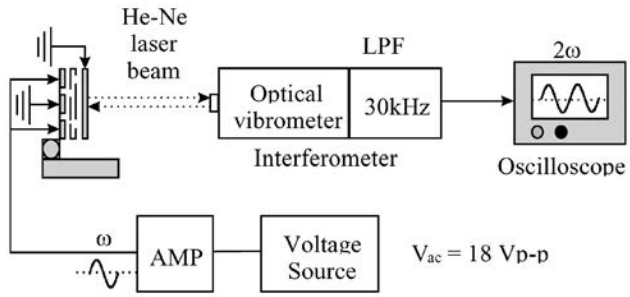

Fig. 6. Velocity measurement of squeeze plate.

The drive voltage frequency was discretely swept from 500 to 30 kHz, while the velocity of the vertical plate motion was monitored. All damping tests were performed at 1 atm and room temperature. We repeated the damping test five times for each test structure.

Values of the experimental damping factor, ζ, were extracted from the damping curves (solid lines in Fig. 7), that minimize the sum of the squared error, SSE, between the theoretical velocity curves and the measured velocity responses (dots in Fig. 7):

$$SSE \equiv \sum_{i=1}^{N} \left(V_i - V_i(\zeta) \right)^2 , \tag{14}$$

where V_i is the ith normalized output voltage and $V_i(\zeta_{ex})$ is the normalized theoretical response for ζ. From the experimental damping ratio, ζ_{ex}, the experimental damping coefficient, b_{ex}, is obtained:

$$b_{ex} = 2\zeta_{ex}\omega\left(2\pi f_n\right)m_e . \tag{15}$$

Figure 8 shows the theoretical Q-factors with the experimental values. In Fig. 8, two different theoretical Q-factors are estimated from FEA with zero-pressure boundary conditions as well as from the matched-asymptotic-expansion analysis with nonzero pressure along the edges of the plate. The experimental Q-factors in Fig. 8 are measured from the damping test structures of the perforated plates (H1, H4, and H9). In Fig. 9, we show the Q-factors of Fig. 8 in terms of the total edge length of the unperforated (H0) and perforated plates.

For the squeeze film damping of the unperforated plate, the finite element solution of Q = 0.27 slightly overestimates the experimental value of Q = 0.18±0.2, whereas the matched-asymptotic-expansion solution of Q = 0.21 shows better agreement with the experimental value. For the perforated plates, the theoretical Q-factors estimated from FEA tend to overestimate experimental values by up to 150% (or underestimate the experimental damping effect), whereas the theoretical Q-factors estimated from matched-asymptotic-expansion are in agreement with the experimental values within 20% margin of

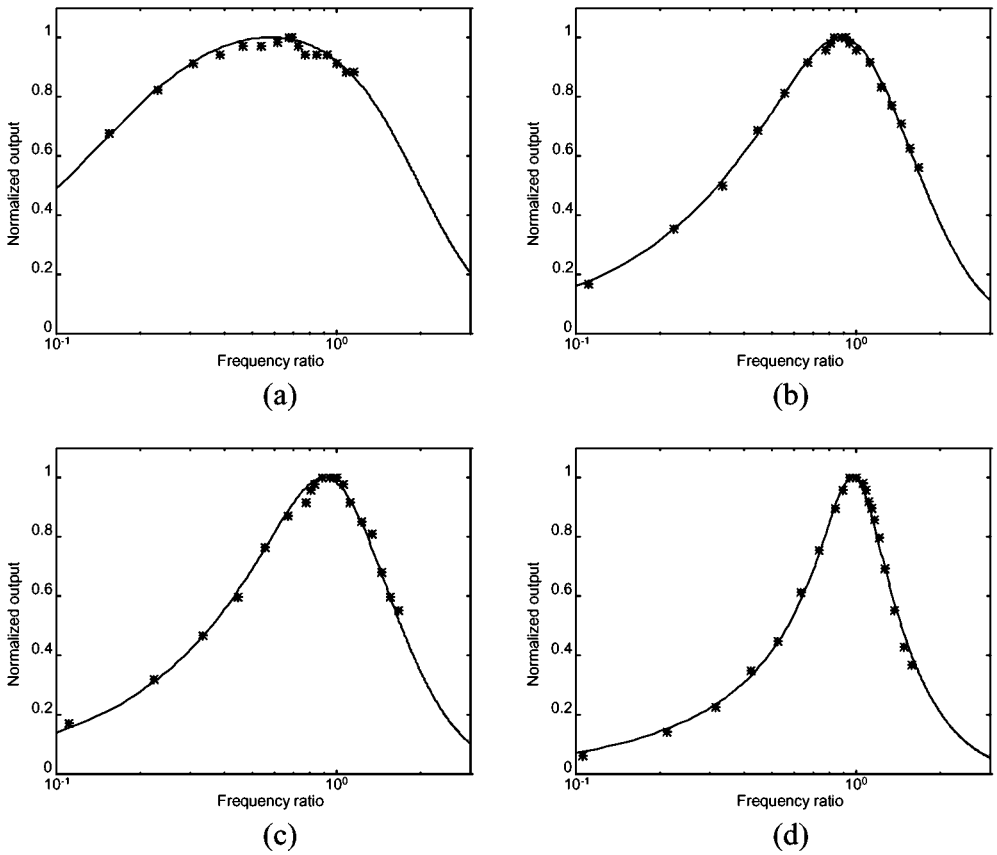

Fig. 7. Extraction of damping factors from least-squares fit of the normalized frequency-dependent velocity response of fabricated plates: (a) H0; (b) H1_AR3.4; (c) H4_AR3.4; (d) H9_AR3.4.

errors. Figure 8 shows that the discrepancy between the finite element *Q*-factors, and experimental *Q*-factors increase as the number or the *AR* of the perforation increases.

In Fig. 9, we find that the discrepancy between the experimental and the finite element results is related to the total edge length of the perforated plate for an identical net-damping area. The matched-asymptotic-expansion solutions, assuming the nonzero pressure along the edges, are in good agreement with the experimental values. We conclude that the major errors in the finite element solutions result from the zero pressure along the edges of plates and perforations. The matched-asymptotic-expansion solutions show that in the squeeze film damping of the perforated plates, the pressure along the edges is nonzero, thus resulting in a larger squeeze damping than the values estimated from FEA.

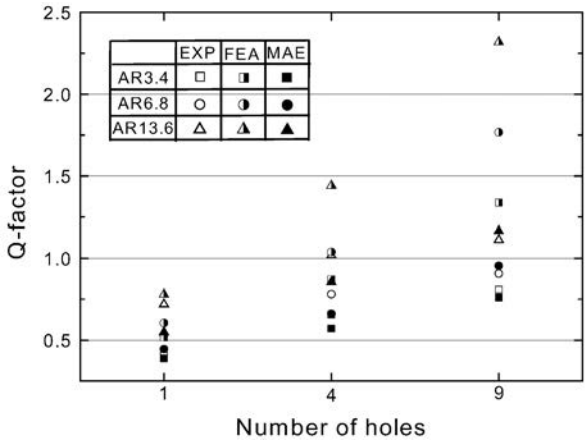

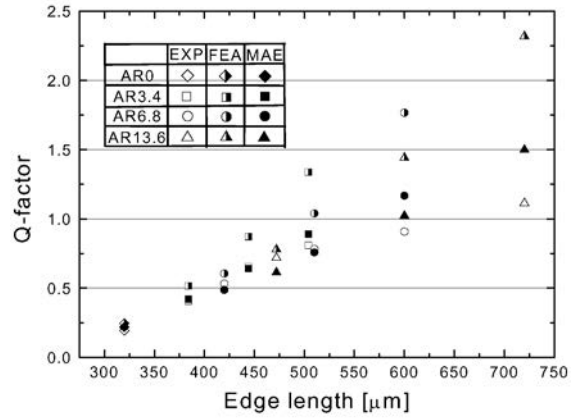

Fig. 8 (left). Theoretical and experimental *Q*-factors for perforated plates of Fig. 3: EXP, FEA, and MAE indicate the experimental values, theoretical values from finite element analysis, and theoretical values from matched asymptotic expansions, respectively.
Fig. 9 (right). Theoretical and experimental *Q*-factors in terms of total edge length of perforated plates of Fig. 3 with identical net damping area: EXP, FEA, and MAE indicate the experimental values, theoretical values from finite element analysis, and theoretical values from matched asymptotic expansions, respectively.

4. Conclusions

We performed a theoretical and experimental study on the viscous damping of perforated planar microstructures that oscillate perpendicular to the substrate. We designed, fabricated, and tested a set of squeeze film dampers, having planar plates with ten different types of perforation. Compared with the measured *Q*-factors, we found that the theoretical *Q*-factors estimated from FEA underestimate the squeeze damping effects, whereas the theoretical *Q*-factors estimated from matched-asymptotic-expansions are in good agreement with the experimental results. The discrepancy between the experimental *Q*-factors and the finite-element solutions tends to increase as the total edge length of the perforated plates increases. By assuming a nonzero pressure along the edges of the perforated plates, the matched-asymptotic-expansion solutions were in good agreement with the experimental *Q*-factors.

Acknowledgement

This study was supported by the National Creative Research Initiative Program of the Ministry of Science and Technology (MOST) and the Korea Science and Engineering Foundation (KOSEF) under the project title of “Realization of Bio-Inspired Digital Nanoactuators.”

References

1 J. Bergqvist and J. Gobert: J. Microelectromech. Sys. **3** (1994) 69.
2 M. J. Novack: Design and Fabrication of a Thin Film Micromachined Accelerometer (M.S. Thesis, Massachusetts Institute of Technology, 1992).
3 J. B. Starr: Tech. Digest IEEE Solid State Sensor and Actuator Workshop (Hilton Head Island, USA, 1990) p. 44.
4 D. Arch, T. Ohnstein, D. Zook and H. Guckel: IEEE/LEOS Summer Topical Meetings (1996) p. 21.
5 M. S. Wu, E. C. Vail, G. S. Li, W. Yuen and C. J. C.-Hasnain: IEEE Photonics Technol. Lett. **8** (1996) 98.
6 M. H. Sadd and A. K. Stiffler: J. Eng. Ind. Trans. ASME **97** (1975) 1366.
7 J. Blech: J. Lubrication Technol. **105** (1983) 615.
8 M. Andrews, I. Harris and G. Turner: Sens. Actuators, A **36** (1993) 79.
9 E.-S. Kim, Y.-H. Cho and M.-U. Kim: 12th IEEE Inter. Conf. Microelectromechanical Systems 1999 (IEEE, Florida, 1999) p. 296.
10 M.-U. Kim, K. W. Kim, Y.-H Cho and B. M. Kwak: Fluid Dynamics Resesrch **29** (2001) 171.
11 J. A. Williams: Engineering Tribology (Oxford, 1994) p. 320.
12 A. F. Mills: Heat Transfer (Irins, Boston, 1992) p. 126.

Appendix Theoretical Analysis

A.1 *Analytic solutions for unperforated plates*

For a small-amplitude motion (Fig. 1), the micromechanical dynamics of the microstructure (Fig. 2) can be considered as a linear system. The dynamic behavior of the micromechanical system is described by the second-order ordinary differential equation

$$m_e \ddot{\chi} + b_e \dot{\chi} + k_e \chi = F\cos(\omega t), \tag{4}$$

where m_e, b_e, and k_e represent the effective mass, effective damping coefficient, and effective stiffness, respectively. In eq. (4), F and ω indicate the amplitude and frequency of the periodic drive force, respectively. The independent variable, χ, is the relative displacement with respect to the equilibrium position.

The dynamic characteristics of the damping test structures are represented by the damping ratio, ζ, and the natural frequency, f_n, respectively defined as

$$\zeta = \frac{b_e}{\sqrt{m_e k_e}}, \tag{5}$$

$$f_n = \sqrt{\frac{k_e}{m_e}}. \tag{6}$$

At resonance, the Q-factor is defined as $Q = 1/2\zeta$.

A fluid film of uniform thickness, d_0, confined between the substrate and the square plate, develops a pressure disturbance when the plate is oscillating perpendicular to the substrate. A nondimensional squeeze number, σ, is defined[11] for the fluid film underneath the plate as

$$\sigma = \frac{12\mu\omega l^2}{{d_0}^2 P_a}, \tag{7}$$

where μ, ω and l are the fluid viscosity, oscillating frequency, and width of the square plate, respectively.

At low squeeze numbers, i.e., less than 0.3,[3] the fluid is squeezed without compression; hence, the fluid stiffness effect is negligible. The squeeze film can be analyzed using the Navier-Stokes equation under the assumption of a small Reynolds number, i.e., less than 1, an isothermal squeeze and a small pressure variation in the fluid film, and a small-amplitude motion compared with the nominal film thickness:

$$\frac{\partial^2 P_d}{\partial x^2} + \frac{\partial^2 P_d}{\partial y^2} = \frac{12\mu}{{d_0}^3}\frac{\partial d}{\partial t}, \tag{8}$$

where d is the fluid film thickneess, x and y are the spatial coordinates, and P_d is the pressure distribution whose boundary conditions are zero along the edges, and zero pressure gradient at the center of the film. The pressure integrated over the plate surface gives the damping force. Thus, the damping coefficient, b, for a perfectly unperforated square plate[2] becomes

$$b = 0.422\frac{\mu l^4}{{d_0}^3}. \tag{9}$$

A.2 *Finite-element solution for perforated plates*

For the perforated plates, a finite element program, ANSYS, is used to estimate the damping coefficients, natural frequencies, and modal shapes of each damping test structure. The damping coefficients and the distribution of the pressure in the squeeze film are analyzed as follows: Reynolds equation for the squeeze film damping pressure, eq. (8), is analogous to the Poisson equation,[12] governing two-dimensional heat conduction for temperature, T:

$$\frac{\partial^2 T}{\partial x^2} + \frac{\partial^2 T}{\partial y^2} = \frac{\dot{q}}{k}, \tag{10}$$

where $\dot{q}$ is the rate of heat generation per unit volume and k is the isotropic thermal conductivity. We apply zero-pressure boundary conditions to the nodes on the edges of the plate and holes for the FEA. We calculate the damping forces from the integration of the pressure over the plate area, from which we obtain the damping coefficient.

A.3 *Matched-asymptotic-expansion solutions for perforated plates*

When the damping gap is much smaller than the characteristic sizes of the plates, the damping coefficients and pressure distribution due to the motion of the unperforated and perforated plates can be estimated by matched-asymptotic-expansion.[10] The pressure distribution underneath the oscillating plate is determined by solving the two equations

$$\frac{\partial^2 P_{-3}}{\partial x^2} + \frac{\partial^2 P_{-3}}{\partial y^2} = 12,\ p_{-3}\big|_{\partial\Omega} = 0, \tag{11}$$

$$\frac{\partial^2 P_{-2}}{\partial x^2} + \frac{\partial^2 P_{-2}}{\partial y^2} = 0,\ p_{-2}\big|_{\partial\Omega} = \frac{C_B}{2}\frac{\partial p_{-3}}{\partial n}\bigg|_{\partial\Omega}, \tag{12}$$

where p_{-3} and p_{-2} are the first- and second-order expressions of the pressure, respectively, expanded in an asymptotic series of $p = \varepsilon^{-3}p_{-3} + \varepsilon^{-2}p_{-2} + \ldots$, $\partial\Omega$ denotes the edge of the plate and perforations, n is the outward normal direction, and $C_B = -1.27$ is a constant determined by the damping gap and structure thickness. Pressure and coordinate variables are nondimensionalized with $\mu W/l$ and l, respectively.

Equation (11) is the well-known Reynolds equation and eq. (12) corresponds to the edge effect, which amounts to a considerable part of the total pressure. Integrating the pressure over the plate, we obtain the damping coefficient on the plate:

$$b = \frac{F}{W} = \mu l \int_\Omega \left(\varepsilon^{-3}p_{-3} + \varepsilon^{-2}p_{-2}\right) dxdy, \tag{13}$$

where Ω denotes the region of the plate except the perforations, F is the normal force on the plate, and W is the characteristic velocity of the plate.

Figures 10 and 11 show the pressure distributions under the unperforated and perforated plates oscillating perpendicular to the substrate, estimated from FEA and matched-asymptotic-expansion,

respectively. From the matched-asymptotic-expansion, we estimate the maximum amplitudes of the pressure along the edges of the plates (Fig. 12) and perforations (Fig. 13). Figures 12 and 13 show that the pressure amplitude along these edges is higher than the zero pressure assumed in FEA.

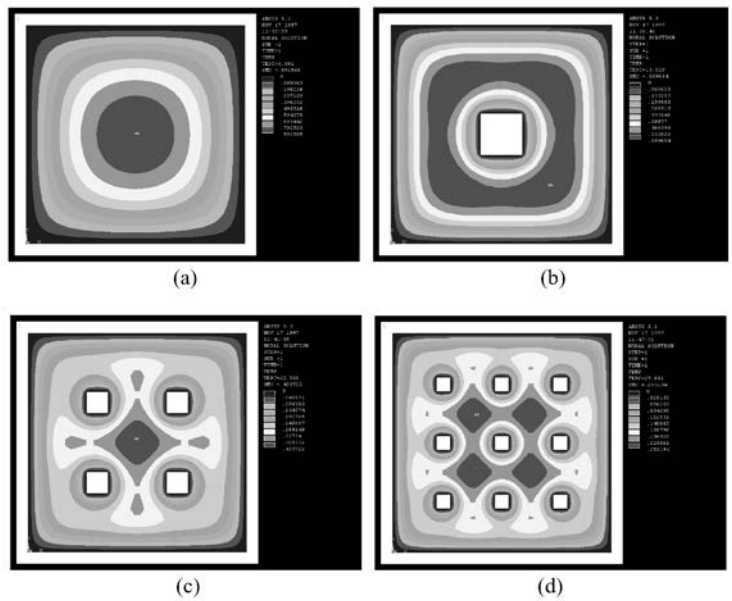

Fig. 10. FEA of squeeze film pressure underneath plates: (a) H0; (b) H1_AR3.4; (c) H4_AR3.4; (d) H9_AR3.4.

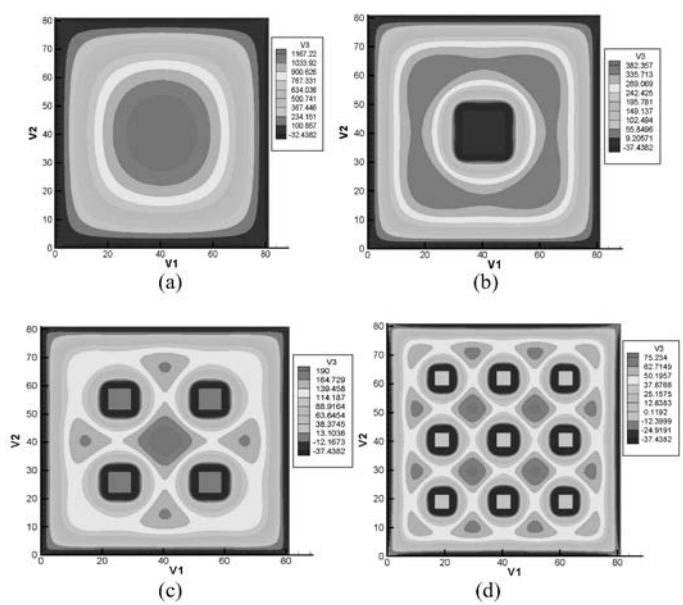

Fig. 11. Matched asymptotic expansions of pressure distribution under plates: (a) H0; (b) H1_AR3.4; (c) H4_AR3.4; (d) H9_AR3.4.

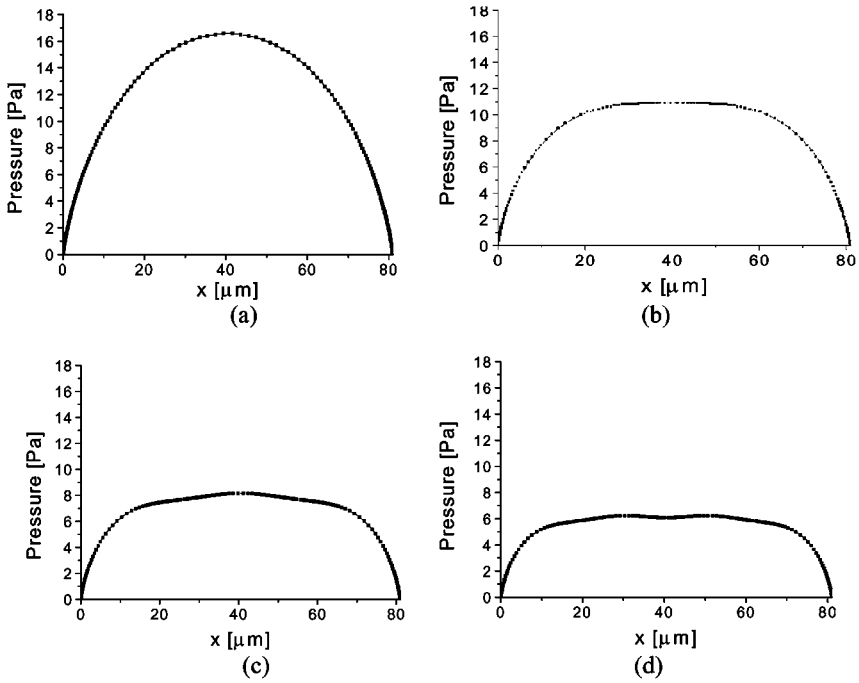

Fig. 12. Pressure amplitude of plate edges under plates, from matched asymptotic expansions: (a) H0; (b) H1_AR3.4; (c) H4_AR3.4; (d) H9_AR3.4.

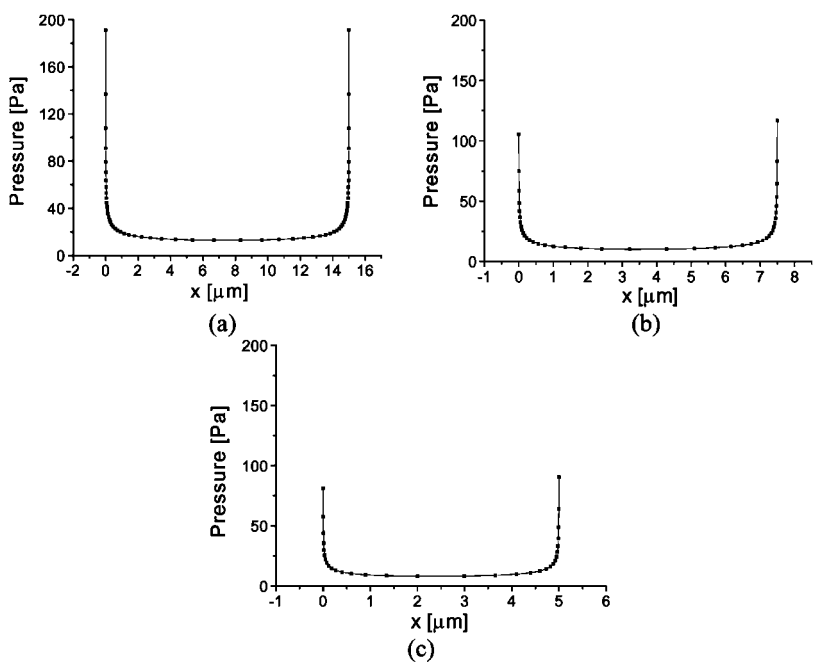

Fig. 13. Pressure amplitude of perforation edges under perforated plates, from matched asymptotic expansions: (a) H1_AR3.4; (b) H4_AR3.4; (c) H9_AR3.4.